Sharifi, M., Forootan, E., Nikkhoo, M., Awange, J., Najafi-Alamdari, M. (2013): A point-wise least squares spectral analysis (LSSA) of the Caspian Sea level fluctuations, using TOPEX/Poseidon and Jason-1 observations. - *Advances in Space Research*, *51*, 5, p. 858-873.

DOI: http://doi.org/10.1016/j.asr.2012.10.001

This is a pre-print version of the original paper:

M.A. Sharifi, E. Forootan, M. Nikkhoo, J.L. Awange, M. Najafi-Alamdari, (2013),
A point-wise least squares spectral analysis (LSSA) of the Caspian Sea level
fluctuations, using TOPEX/Poseidon and Jason-1 observations,
Advances in Space Research, Volume 51, Issue 5, 1 March 2013,
Pages 858-873, ISSN 0273-1177, http://dx.doi.org/10.1016/j.asr.2012.10.001.

(http://www.sciencedirect.com/science/article/pii/S0273117712006345)

Keywords: Caspian Sea level; TOPEX/Poseidon; Jason-1; Least squares
spectral analysis (LSSA); PCA

A point-wise least squares spectral analysis (LSSA) of the Caspian Sea level fluctuations, using Topex/Poseidon and Jason-1 observations

M. A. Sharifi[a], E. Forootan[b,1], M. Nikkhoo[c], J. L. Awange[d,e], M. Najafi-Alamdari[f]

[a] *Surveying and Geomatics Engineering Department, University of Tehran, Iran*
[b] *Institute of Geodesy and Geoinformation (IGG), Bonn University, Nussallee 17, Bonn, Germany*
[c] *Department of Physics of the Earth, Helmholtz Centre, GFZ Potsdam, Telegrafenberg 14473, Potsdam, Germany*
[d] *Western Australian Centre for Geodesy and The Institute for Geoscience Research Curtin University, Perth, Australia*
[e] *Geodetic Institute, Karlsruhe Institute of Technology (KIT), Karlsruhe, Germany*
[f] *Geodesy and Geomatics Engineering Department, K.N. Toosi University of Technology, Tehran, Iran*

Abstract

The Caspian Sea has displayed considerable fluctuations in its water level during the past century. Knowledge of such fluctuation is vital for understanding the local hydrological cycles, climate of the region, and construction activities within the sea and along its shorelines. This study established a point-wise satellite altimetry approach to monitor the fluctuations of the Caspian Sea using a complete dataset of TOPEX/Poseidon for the period 1993 to the middle of 2002, and its follow-on Jason-1 for the period 2002 to August 2009. Therefore, 280 virtual time-series were constructed to monitor the fluctuations. The least squares spectral analysis (LSSA) method is, then employed to find the most significant frequencies of the time-series, while the statistical method of principle component analysis (PCA) is applied to extract the dominant variability of level variations. The study also used the observations of TOPEX/Poseidon and Jason-1 over the Volga River along with 5 years of Volga's water discharge to study its influence on the Caspian Sea level changes. The LSSA results indicate that the lunar semidiurnal (M2) and the Sun semidiurnal (S2) frequencies are the main tidal frequencies of the Caspian Sea with the mean amplitude of 4.2 and 2.8 cm, respectively. A statistically significant long-term frequency (12.5-

Email addresses: sharifi@ut.ac.ir (M. A. Sharifi), forootan@geod.uni-bonn.de (E. Forootan), mehdi.nikkhoo@gfz-potsdam.de (M. Nikkhoo), J.Awange@curtin.edu.au (J. L. Awange), mnajalm@yahoo.com (M. Najafi-Alamdari)

[1] Address for corresponding author (Ehsan Forootan): Institute of Geodesy and Geoinformation, Bonn University, Nussallee 17, D53115, Bonn, NRW, Germany, Tel: 0049228736423, Fax: 0049228733029, E-mail: forootan@geod.uni-bonn.de

years period) is also found from altimetry and tide gauge observations. A phase lag, related to the inter-annual frequencies of the Volga River was detected from the point-wise time-series showing level propagation from the northwest to the southeast of the sea. The Cross-correlation between the power spectrum of Volga and that of the northern-most, middle, and southern-most points within the Caspian Sea were respectively 0.63, 0.51 and 0.4 of zero-lag correlation, corroborating the influence of the Volga River. The result of PCA also shows that different parts of the Caspian Sea exhibit different amplitudes of level variations, indicating that the point-wise approach, when employing all available satellite measurements could be a suitable method for a preliminary monitoring of this inland water resource as it gives accurate local fluctuations.

Key words: Caspian Sea level, TOPEX/Poseidon, Jason-1, least squares spectral analysis (LSSA), PCA.

---

1. Introduction

The Caspian Sea (Fig. 1), situated between latitudes 36.5°N and 47°N and longitudes 46.5°E and 54.5°E is the world's largest inland water body with an area of about 400,000 km^2, stretching approximately 1,200 km long in the north-south direction (e.g., Dumont, 1998; Rodionov, 1994). Its width ranges from 435 km to a minimum of 196 km, while its length is divided into three sub-basins (the most northern, the middle, and the southern parts). Most of the northern Caspian is shallow, with an average depth of 4 m. The average depth increases southwards with it being about 800 m around the central and approximately 1 km in the southern part (Dumont et al., 2004). The Caspian Sea has no connection to the world's oceans and its surface level is around -26.5 m below Mean Sea Level (MSL) (Kosarev, 2005; Kouraev et al., 2011).

During the last century, the Caspian Sea displayed considerable fluctuations in its water levels, which have been the subject of several studies (e.g., Rodionov, 1994; Kosarev and Yablonskaya, 1994; Swenson and Wahr, 2007; Lebedev and Kostianoy, 2005, 2006, 2008a,b, 2010; Kouraev et al., 2011). Ignatov et al. (1993), for example, explained the cause of these fluctuations to be possibly climatic, and that it is dependent on the water budget of its basin (precipitation and river recharge minus water loss by evaporation). Impact of ice coverage changes on the level variations of the Caspian and its detecting using altimetry data sets is discussed, e.g., in Kouraev et al. (2003, 2004 and 2008). Short-term wind-induced fluctuations are known to cause a rise of up to 4 m, although the average fluctuation is about one meter. Other causes include; barometric pressure, tidal variations (often less than 1 m), and seasonal rises induced by high rates of water flow during spring water in the rivers. For more information about physical and geo-physical aspects of the region, see e.g., Kosarev (2005) and Kouraev et al. (2011). Indeed, fluctuations of inland water bodies are sensitive to climate change and serve as one of its indicators, as was demonstrated in the case of Lake Victoria in East Africa, e.g., by Awange et al. (2008) and

the Caspian Sea e.g., by Kouraev et al. (2011).

On the one hand, the Caspian Sea level changes play a vital role in indicating regional climate change given its three micro-climatic basins (Dumont, 1998; Kouraev et al., 2011)). Its flooding on the other hand could lead to environmental and economic damage as was the case following its sudden rise in 1978 (Ignatov et al., 1993, Cazenave et al., 1997). Moreover, Caspian's fluctuations have been shown, e.g., by Ignatov et al. (1993) to be cyclic over 30-50 years, thereby prompting Ignatov et al. (1993) to warn that if the cyclic pattern is true, a further rise of its water level should be expected in the near future. Knowledge of the fluctuation of its water level, therefore, is not only vital as an indicator of the changing climate, but also to inform environmental flood management programs, thus necessitating the need for continuous monitoring of variations in its level.

Long-term (century-scale) fluctuations of Caspian Sea have been reconstructed from archaeological, geographical, and historical data. The task has been compounded by its sheer size, which makes determining its average water level more complicated. Long-term records show that the average level has varied considerably over the last century, and many studies have been undertaken to attempt to predict mean water-level variations (e.g., Georgievskiy, 2001 and the references therein). Monitoring changes in the water level of inland water bodies the size of the Caspian Sea requires an accuracy and completeness of geographical data coverage that challenges conventional measurement capabilities such as tide gauges.

To meet this challenge, in recent years, space-based remote sensing has provided essential new information. One example is the TOPEX/Poseidon (T/P) mission, a satellite altimetry approach that was designed to precisely monitor absolute sea level changes (e.g., Minster et al., 1995; Nerem, 1995; Cazenave et al., 1997), but also found application in monitoring inland lake level changes (e.g., Birkett, 1994, 1995; Shum et al., 2003; Crétaux and Birkett, 2006). T/P was applied, e.g., by Cazenave et al. (1997) to monitor the Caspian Sea level from January 1993 until August 1996 (i.e., 3.5 years), from which a fall in its level was shown. Kostianoy and Lebedev (2006) and Lebedev and Kostianoy (2008a,b) studied the level fluctuation using nine points located on the cross-tracks of T/P and Jason-1. Swenson and Wahr (2007) used satellite altimetry (Jason) together with the GRACE (Gravity Recovery And Climate Experiment) products to analyze the water storage variation of the Caspian Sea from mid 2002 to 2006, and provided a means by which indirect satellite data could be validated.

Due to the vast size of the Caspian Sea, and the varying climatic patterns within the whole sea (discussed in Sec. 2), each region of the sea would be expected to have a water level pattern different from the other regions. In such a case, it will be desirable to have a method that would provide an analysis of each region individually. A common feature in most of the studies mentioned above, however, is that the Caspian Sea has been treated as a whole, where a single point variation was determined, e.g., in Swenson and Wahr (2007) and Crétaux et al. (2011) or the investigated points were constrained to the cross

over of altimetry satellites, e.g., in Lebedev and Kostianoy (2005, 2006, 2008a,b and 2010). In a recent study of Kouraev et al. (2011), though, the spatio-temporal variability of the Caspian Sea is assessed. The spectral characteristics of level variations of the Caspian Sea is, however, is not considered in Kouraev et al. (2011).

This contribution, therefore, extends these previous studies, by investigating point-wise time-series that looks at the various regions of the Caspian Sea, in addition to treating it as a whole. The data used in this study consists of the T/P mission spanning from 1993 to September 2002 and JASON-1 from 2002 to August 2009, which are employed to generate 280 reliable time-series of sea level changes that cover all the sea surface. In order to extract the spectral characteristics of each time-series, this study employed the least squares spectral analysis (LSSA) (Vaníček, 1969) to obtain the main frequencies of sea level changes. From these frequencies, a Fisher statistical test is undertaken to determine the significant frequencies which are then compared to those frequencies of celestial tides as well as the Volga River discharge to explore their influences on each region. Besides, the statistical method of principle component analysis (PCA) is used to extract and visualize the main variability of sea level changes after removing the tidal frequencies.

The remaining part of the paper is organized as follows: in the next section, we briefly describe the Caspian Sea. The data used in the study is presented in Section 3, while Section 4 outlines the analysis methods, and the results are presented and discussed in Section 5. Finally, Section 6 summarizes the major findings.

2. The Caspian Sea

The Caspian Sea (Fig. 1) is supplied mainly by discharge from rivers and precipitation. Its water budget is completed by being drained predominantly through evaporation and a minor outlet to Kara-Bobaz Gulf. The largest of these rivers is the Volga, which drains an area of 1,400,000 km^2 and runs into the north-western part of the Caspian, contributing more than 80% of the total inflow (Dumont, 1998). The Volga River, together with Kura, Terek, Ural and Sulak, supply over 90% of the inflowing freshwater to the Caspian Sea. The Iranian rivers and smaller streams on the north-eastern part of the country supply the remaining 10%, since there are no permanent inflows on the eastern side (e.g., Kazakhstan and Turkmenistan regions) (TDA, 2002).

The average salinity of the sea is about 12.8 psu, which is almost three times lower than what is normally found in the open oceans, especially in the northern Caspian, where there is a large inflow of fresh water from the Volga and Ural rivers. Ice forms in the northern portions of Caspian in early November and reaches its maximum southern extent by January or February (Kosarev and Yablonskaya, 1994).

The climatic conditions of the Caspian Sea are influenced by cold Arctic air, moist sea air masses forming over the Atlantic ocean, dry continental air masses from Kazakhstan, and warm air masses coming from the Mediterranean

Sea and Iran. According to Rodionov (1994), three types of the atmospheric circulation over Russia exist. Among them, the meridian type, which is characterized by stable high pressure over European Russia, resulting in cold winters and hot cloudless summers, is most common and has been more dominant than usual over the Caspian Sea in recent years (Kosarev, 2005). Extreme temperature conditions contribute to the changing Caspian Sea level while the annual component has an amplitude of approximately 20 mm as reported in Swenson and Wahr (2007). A detailed discussion on the ice cover of the Caspian Sea as well as the techniques for detecting them from remote sensing observations are documented, e.g., in Kouraev et al. (2003, 2004 and 2008).

FIGURE 1

3. Data

Three datasets were used in this study. These are (i) derived water levels from T/P and JASON-1 satellite altimetry missions, (ii) water levels from tide gauge in-situ measurements provided by the Iranian Caspian Environmental Study Center, and (iii) the Volga River discharge.

3.1. TOPEX/Poseidon (T/P) and JASON-1 altimetry data

The launching of the T/P mission on the 10th of August 1992 opened a new era for understanding global ocean dynamics by making precise and accurate observations of sea level variation. The satellite covered the Earth from 66 °N to 66 °S which includes most of the ice-free oceans. The T/P satellite orbited at an altitude of 1,336 km above the reference ellipsoid (a mathematical figure approximating the mean sea level) and measured the distance between the satellite and the Earth's sea surface with an accuracy of 4 cm (Birkett, 1995). JASON-1 was launched as the follow-on mission to the T/P on the 7th December of 2001 and overflies nearly the same ground-tracks (Picot et al., 2003).

Each of T/P and JASON-1 cycles includes 254 passes, where 127 are ascending and 127 are descending. In most of them, eight ground tracks pass through the Caspian Sea with reliable altimetry, as shown in Fig. (1). To obtain the SSH of the Caspian Sea during more than ten years (1993-2003) of the T/P mission, its cycles (11th to the 365th) in the form of *Merged Geophysical Data Record* (MGDR) are used. For JASON-1, use is made of 283 cycles of the Interim Geophysical Data Record (IGDR) from the NASA Physical Oceanography Distributed Active Archive Center (PODAAC) at the Jet Propulsion Laboratory (JPL) of California Institute of Technology. Note that MGDRs and IGDRs represent more accurate altimetry data of the T/P and JASON-1 missions, respectively (see e.g., Kouraev et al., 2011). In this study, however, the data of MGDR and IGDR are used to make the results comparable to those of previous studies, e.g., Kostianoy and Lebedev (2006) and Lebedev and Kostianoy (2008a,b).

In general, each MGDR and IGDR file incorporates improved orbits (Nerem et al., 1993) that yield satellite heights from a reference ellipsoid. The main

component of both datasets is the altimetric ranges measured at the Ku and C bands. We used the Ku band range data, which is recommended for most applications (e.g., Benada, 1997). The provided ranges are already corrected for instrumental effects such as drifts. However, they must be corrected for the atmospheric errors (e.g., ionospheric and tropospheric effects), which affect the radar pulse as it passes through the atmosphere, and the nature of the reflecting sea surface. The corrected range is calculated following the handbook of products (Benada, 1997; AVISO, 1996)

$$\rho^{c} = \rho + \Delta w + \Delta d + \Delta I + \Delta IB + \Delta E + \Delta PT + \Delta CM, \quad (1)$$

where ρ^{c} and ρ are the corrected and measured range values respectively, Δw, Δd and ΔI are the wet tropospheric, dry tropospheric and ionospheric corrections, respectively. Electromagnetic bias and inverse barometer errors are corrected by the terms ΔE and ΔIB, respectively. Corrections due to temporal variations in the used coordinate system, i.e., the geocentric pole tide and center of gravity motions, are given by the terms ΔPT and ΔCM, respectively. All of the correction parameters in Eq. (1) are included in the provided MGDR and IGDR data.

Since the tidal model used in the MGDR and IGDR products are valid only for the oceans (Benada, 1997; AVISO, 1996), their associated corrections were not applied to correct the ranges (Eq. (1)), at this stage. However, for the Caspian Sea that exhibits a non-neglectable tidal fluctuations, the tidal corrections needed to be computed from a regional tidal model or the data itself (AVISO, 1996; Kouraev et al., 2011). In this study, once the point-wise time-series were computed in Section. 3.1.1, the tidal coefficients of the Caspian Sea were derived from the LSSA of each point-wise time-series and used to correct each observation (discussed in Sec. 5.2).

Kouraev et al. (2011) state that the dry and wet tropospheric corrections, included in the MGDR and IGDR products, are not correctly computed. Therefore, they suggest a use of a best possible model e.g., ECMWF (Mercier and Zanife, 2006), to compute the corrections. This study, however, used the flag from Brown (2010) to exclude those observations with invalid correction values. In order to estimate the impact of using different corrections (in Eq. (1)) on the desired SSH measurements over the Caspian Sea, we compared the most uncertain corrections (including dry tropospheric, wet tropospheric, and inverse barometric corrections) to those corrections derived from the ECMWF atmospheric model. The corrections of ECMWF were downloaded from the Radar Altimeter Database System of Delft University of Technology [1]. Fig. 2 shows that the magnitude of differences between their standard deviations, after using the mentioned flag, reaches up to 5 cm which are mainly concentrated over the southern coasts.

[1] http://rads.tudelft.nl/rads/rads.shtml

FIGURE 2

After correcting the data according to Eq. (1), the instantaneous ellipsoidal height of sea surface (SSH) is computed by the difference:

$$\mathrm{SSH}(\phi, \lambda, t) = H_{\mathrm{sat}}(\phi, \lambda, t) - \rho^{\mathrm{c}}(\phi, \lambda, t), \tag{2}$$

where $H_{\mathrm{sat}}(\phi, \lambda, t)$ is the altitude of the satellite at a given location and time measured from the reference ellipsoid provided in MGDR and IGDR datasets.

In addition to the mentioned SSH products, we used the SSH products of Crétaux et al. (2011) to validate our computations. Crétaux et al. (2011) used the environmental satellite (ENVISAT) measurements in addition to T/P and JASON-1 for computing SSHs over the Caspian Sea. Their results can be found from the official website of the Laboratoire d´Etudes en Géophysique et Océanographie Spatial (LEGOS) [2].

In order to derive the surface heights above the geoid, following Cazenave et al. (1997), the averaged collinear passes of T/P over complete ten years of 1993-2002 were considered as the geoid of the Caspian Sea. SSH at each point then referred to the geoid by computing the difference of Eq. (2) and the 10-year mean level of that point. The priority of using a suitable mean sea level instead of geoid models for reducing SSH of the Caspian Sea is also addressed in Kouraev et al. (2011).

3.1.1. Point-wise SSH *time-series*

Since T/P and JASON-1 orbit the Earth in a repeat mode, the footprints of satellites from different cycles are located in close proximity. Consequently, one can interpret each altimetry point as a virtual tide gauge where the sea surface height is observed every 9.915625 days. From this perspective, satellite observed sea heights can be independently analyzed for each observation location which is called here the 'Point-wise' approach.

However, satellites do not repeat exactly at the same ground track. Differences between tracks (footprints) are around 1 km (Hwang et al., 2005). Therefore, it is necessary to map repeated sea level observations of different cycles to a reference cycle. While the separation between every two sequential measurements in one pass is around 5 km, we treat all the observations from *cycle* 011 of T/P as the reference points. Then, those observations from other cycles of T/P and JASON-1 that were located within a radius of 3 km to the reference points were considered as repeated observations.

It should be mentioned here, that the definition of the detected points as time-series introduces a problem, that is, different cycles have a different geoid profile. This effect is called the cross-track geoid gradient and has a non-negligible influence on SSH (Benada, 1997). The problem is solved by reducing the SSH of the detected points by the geoid difference to the reference point.

[2] http://www.legos.obs-mip.fr/en/soa/hydrologie/hydroweb/Page_ 2.html

The bias between SSHs of the two missions is also removed by implementing a simple shift, while assuming those of T/P tracks as the reference (see also Chambers et al., 2003).

Using the point-wise approach, 280 virtual time-series with reliable records are computed over the Caspian Sea. SSH time-series of the three points, i.e., the northern-most (44.86 °N and 48.01 °E), middle (42.28 °N and 50.16 °E), and southern-most (37.59 °N and 53.54 °E) points of Fig. 1, are shown in Fig. 3. The time-series are corrected for the tidal main frequencies (Table. 1) using LSSA (Eq. 5), with the correction procedure described in Sec 5.2. The middle graph also compares the derived SSH time-series of the middle point with the results of Crétaux et al. (2011) [3] for a virtual point located in 42 °N and 50 °E, showing high agreement.

FIGURE 3

It is necessary to mention that the computed time-series in the point-wise approach depicts the behavior of sea level variations only at that single position and its surrounding, and cannot be generalized to other locations of the sea. Furthermore, due to the variations caused by external factors (e.g. the discharge of the Volga River in the north or atmospheric conditions), every location experiences a different phase relationship. This will be discussed in details in Section. 5.4.

3.2. Tide-gauge data

Gil and de Toro (2005) state that recording sea level changes at a fixed location for a suitable period of time can be used to determine the sea surface harmonic oscillation generated by harmonic forces via the harmonic analysis scheme. Therefore, obtaining frequencies from gauge observations is also a reliable method of evaluating the frequencies resulting from the spectral analysis of space-borne sea surface heights (SSH). Lyubushin et al. (2004) previously used the tide gauge datasets around the Caspian Sea to evaluate the level frequencies from 1977 to 1991. Their study, however, does not incorporate the satellite observation, which also provide dense collection of observations all over the sea.

Gauge observation has a relatively long history in BANDAR-E ANZALI (a harbour town on the Caspian Sea, in the Iranian province of Gilan (Bird, 2010). The gauge station is located in the south-western part of the Caspian Sea at 37.47 °N and 49.46 °E (Fig. 1). This study used daily tide gauge records of the ANZALI port from 1983 to 2006 to evaluate the results of the satellite time-series that were located close to this station (see Fig. 4). We also used monthly observations of two other tide gauges in the Iranian coast located at 36.84 °N and 53.27 °E (in Neka) as well as 36.65 °N and 51.50 °E (in Noshahr), covering the period of 1998 to 2008.

[3] The results of Crétaux et al. (2011) are derived from the LEGOS website in http://www.legos.obs-mip. fr/en/soa/hydrologie /hydroweb/StationsVirtuelles/SV_Lakes /Caspian.html

The altimeter results, shown in Fig. 4,top correspond to a location with latitude 37.54°N and longitude 50.74°E, derived from the point-wise analysis discussed in Section. 3.1.1 and corrected for the tidal main frequencies (Table. 1) using LSSA in (Eq. 5). The correlation coefficient between the satellite SSH and Anzali tide gauge observation for the period 1993 to 2007 was 0.86, thus showing a reliable agreement. The closest SSH time series to the location of Neka and Noshahr tide gauges were also extracted. The results show a significant correlation of 0.82 and 0.76 between altimetry and the in-situ values of Neka and Noshahr tide gauges, respectively. The magnitude of the altimetry-derived SSH is about 90% of the gauge observations, which might be due to the instrumental corrections.

FIGURE 4

3.3. Volga River data

Traditionally, the Volga River basin is subdivided into three parts according to the general climatic background characteristics: northern (from northern margins down to approximately the latitude of Saratov), the central or middle part of the basin (approximately from Saratov to Volgograd), and the southern (approximately from Volgograd to southern margins along the Caspian Sea shores and the Kazakhstan border) (Golosovand and Belyaev, 2010).

Since the discharge of the southern basin directly affects the sea level of Caspian, here, we used the available monthly discharge data from 1999 to 2005 measured at the Volgograd hydro-electric power station located upstream from where the Volga flows into the Caspian Sea (Fig. 1).

Further, the measurements of T/P and JASON-1 on the southern Volga are used to study its effect on the sea level fluctuations. Possibility of such study was previously reported in Lebedev and Kostianoy (2006) where they found a significant correlation coefficient of 0.83 for annual and 0.71 for monthly values during the period of January 1992 to December 2003, between the computed satellite time-series and the discharge at the Volgograd power station. Additionally, we validated our time-series over the Volga with the products of the LEGOS [4]. The results are shown in Fig. 5, where the correlation coefficient between the SSH of Volga and its discharge for the period 1999 to 2005 was 0.73.

4. Methodology

4.1. Least Square Spectral Analysis (LSSA)

The least squares estimation technique is a frequently used method for deterministic modeling of measurements (Vanićek, 1969). For a periodic observable, the deterministic part consists of a limited number of periodic components,

[4] http://www.legos.obs-mip.fr/en/soa/hydrologie/hydroweb/Cartes/Volga_Env_Vals.html

which can be modeled by sine and cosine base functions (Vanićek and Krakiwsky, 1986; Foster, 1996). The least squares estimation is employed to decompose any measured observable to its periodic components, which is equivalent to traditional power spectral density determination methods (e.g., Fourier analysis). However, the traditional Fourier analysis is significantly limited in their applications while it requires equally spaced data in the argument. This is almost a seldom case in practice since, observations are usually unequally spaced and scattered (Vityazev, 1996; Rubin, 2002).

To use a traditional spectral analysis such as Fourier analysis, therefore, the unequally spaced original data should be mapped to an equidistant grid. Depending on the smoothness of the original series, the presence of data gaps, and the subjective choice of the mapping function, a new set of observations are generated. The problem is even more critical if one maps the data by interpolation schemes, which also tend to smooth out any high frequency components of the original data series.

To overcome these limitations, Vanićek (1969) developed a method of spectrum computation on the basis of least squares estimation. The method is known as *Least Squares Spectral Analysis (LSSA)* and has been widely applied in geosciences, see e.g., Wu et al. (1995); Craymer (1998).

Assume $\mathbf{f}$ to be an $n \times 1$ observation vector, which contains sea surface hight measurements from satellite altimetry or tide gauge. Then, consider a set of real and positive frequencies $\{\omega_1, \omega_2, \cdots, \omega_m\}$, whose spectral values for a given observation vector are to be determined. For each frequency ω_i, $\boldsymbol{\phi}^{\mathrm{c}}(\omega_i)$ and $\boldsymbol{\phi}^{\mathrm{s}}(\omega_i)$ are defined as the base functions

$$\boldsymbol{\phi}^{\mathrm{c}}(\omega_i) = \begin{pmatrix} \cos\omega_i t_1 & \cos\omega_i t_2 & \cdots & \cos\omega_i t_n \end{pmatrix}^T \tag{3}$$

$$\boldsymbol{\phi}^{\mathrm{s}}(\omega_i) = \begin{pmatrix} \sin\omega_i t_1 & \sin\omega_i t_2 & \cdots & \sin\omega_i t_n \end{pmatrix}^T, \tag{4}$$

where $t_1, t_2, \cdots, t_n$ are the observations times, and could be either equally or unequally spaced measurement epochs. The vectors $\boldsymbol{\phi}^{\mathrm{c}}(\omega_i)$ and $\boldsymbol{\phi}^{\mathrm{s}}(\omega_i)$ construct a design matrix $\boldsymbol{\phi}(\omega_i) = [\boldsymbol{\phi}^{\mathrm{c}}(\omega_i) \;\; \boldsymbol{\phi}^{\mathrm{s}}(\omega_i)]$.

Therefore, as in Vanićek (1969), the spectral value of each frequency can be computed from

$$S(\omega_i) = \frac{\mathbf{f}^T \boldsymbol{\phi}(\omega_i)(\boldsymbol{\phi}^T(\omega_i)\boldsymbol{\phi}(\omega_i))^{-1}\boldsymbol{\phi}^T(\omega_i)\mathbf{f}}{\mathbf{f}^T\mathbf{f}}. \tag{5}$$

Finally, the set of all these spectral values for all frequencies is called the *least squares spectrum* of the observation vector $\mathbf{f}$, as

$$\mathbf{s}(\boldsymbol{\omega}) = \{S(\omega_1), S(\omega_1), \cdots S(\omega_m)\}. \tag{6}$$

4.1.1. Statistical test

The significance of the estimated spectral values can be tested statistically, thus providing one of the main advantages of the least squares spectral analysis. Steeves (1981) showed that the criteria for accepting or rejecting the null hypothesis, $H_0 : S(\omega_i) = 0$, is defined as:

$$S(\omega_i) = \begin{cases} \leq \left(1 + \frac{\nu}{2} F_{\nu,2,\alpha}\right)^{-1} & ; \quad \text{Accept } H_0 \\ \\ > \left(1 + \frac{\nu}{2} F_{\nu,2,\alpha}\right)^{-1} & ; \quad \text{Reject } H_0, \end{cases} \tag{7}$$

where $F_{\nu,2,\alpha}$ is the critical value of Fisher distribution with ν and 2 degrees of freedom at a significance level of $1 - \alpha$. The results of the statistical tests provided in this study correspond to a 95% level of confidence ($\alpha = 0.05$).

4.1.2. Aliasing phenomenon

According to the Nyquist-Shannon sampling theorem (Shannon, 1984), the maximum detectable frequency of a continuous function, which is sampled equidistantly in n points with spacing Δt, is

$$\nu_{\max} = \frac{1}{2\Delta t} = \frac{n}{2T} = \frac{n}{2}\nu_0, \tag{8}$$

where $T = t_n - t_1$ and ν_0 are the length of the observation time-series and the fundamental or natural frequency, respectively, and $\nu_{\max}$ is the Nyquist frequency (e.g., Awange et al., 2008).

A continuous time-series can only be completely reconstructed from sampled values if the sampling time interval is smaller than $\frac{1}{2\nu_{\max}}$. Otherwise, the period of the component of signal with a frequency of ν aliases to $\nu_{\rm a}$. Therefore, for T/P and Jason1 data with a temporal resolution of 9.915625 days, some of the tidal frequencies with periods less than 10 days will be aliased. According to Wang (2004), for an actual tidal frequency ν^k, there is an aliased frequency $\nu_{\rm a}^k$ such that

$$\nu_{\rm a}^k = |\mathrm{mod}\left(\nu^k + \frac{\nu_{\rm s}}{2}, \nu_{\rm s}\right) - \frac{\nu_{\rm s}}{2}|, \tag{9}$$

where $\nu_{\rm s}$ is the sampling frequency of satellite altimetry. The length of the observation vector should be long enough so that two close tidal components, ν_1 and ν_2 can be separated. This involves determining the Raylight period $T_{\rm r}$ which is defined as,

$$T_{\rm r} = |\frac{\nu_1}{2\pi} - \frac{\nu_2}{2\pi}|, \tag{10}$$

where π is equal to 3.14 and ν_1 and ν_2 are two neighboring frequencies. In order to separate the ν_1 and ν_2, observation period should be larger than the Raylight period. Consequently, we are able to determine all the main tidal frequencies (except the 18.6 years of the moon) using 3 years of T/P or Jason1 observations. Moreover, two marginal Sun semidiurnal and Sun semiannual frequencies are able to be separated if we use 9 years of T/P observations. Therefore, we could expect to sense nearly all tidal components using a decade ($1993 - 2003$) of satellite altimetry data, cf. Wang (2004).

4.2. Principle Component Analysis (PCA)

Principal component analysis (PCA) is a simple, non-parametric statistical method, which can be used for extracting the dominant variability of spatio-temporal data sets (Preisendorfer, 1988). In principle, PCA decomposes a centered matrix $\mathbf{F}$, which in our case contains the 280 SSH time-series of Section 3.1.1 in its columns, in terms of a new set of spatially orthogonal vectors (EOFs) associated with temporally uncorrelated temporal components known as principle components (PCs) (Preisendorfer, 1988).

$$\mathbf{F} = \bar{\mathbf{P}}\mathbf{E}^T, \tag{11}$$

where $\bar{\mathbf{P}}$ contains scaled PCs, i.e. $max(\mathbf{P}) = 1$ and $min(\mathbf{P}) = -1$, and $\mathbf{E}^T = \mathbf{P}^T\mathbf{F}$ contains the corresponding orthogonal spatial patterns in its columns. Ordering orthogonal components (EOFs and PCs) w.r.t the variance of EOFs, the PCA method captures the maximum variability of the data set ($\mathbf{F}$) in a few components (Preisendorfer, 1988). PCA will be used in Section 5.3 to extract the dominant variability of sea level changes within the Caspian Sea.

5. Numerical Results and Discussion

5.1. Trend analysis

Decomposition of the data series to the trends and residuals can be carried out only if the analytical model of the trend is stipulated. This means that the systematic behavior of the measurements is known with respect to the coordinates (in this case, time). It is necessary to remark that the term trend is loosely defined in this work as a long-term change in the mean level. A difficulty with this definition is deciding what is meant by a long-term, i.e., some climatic phenomena exhibit cyclic variations with a very long period. Nevertheless, in the short term, it may still be more meaningful to think of such a long-term oscillation as a trend. Chatfield (1989) defines trend as comprising all cycle components whose wavelength exceeds the length of observed time-series. This definition is adopted for our analysis.

Defining trend in the Caspian Sea is too complicated. Long-term in-situ observations in the Caspian Sea illustrate a nonlinear trend. However, Lyubushin et al. (2004), for example, considered a linear form to model the trend of Caspian Sea level variations before 1995. Based on the results of Fig. 3), however, it is clear that the behavior of the Caspian Sea water level has changed compared to the time before 1995.

In order to model the trend in each satellite time-series, we considered a nonlinear trend based on the least squares polynomial fit in the form of $ssh = at^n + bt^{n-1} + ... + c + e\cos(2\pi f_1 t)) + f\sin(2\pi f_1 t)) + g\cos(2\pi f_2 t) + h\sin(2\pi f_2 t)))$. Where ssh is the observed level height, t time of observation, n the maximum degree of polynomial, f_1 the annual, and f_2 the semi-annual frequencies. The unknown coefficients ($a, b, ..., c, e, f, g$ and h) are estimated using a least squares adjustment (Vanićek and Krakiwsky, 1986).

Our analysis shows that for most of the time-series (except for the time-series over the Kara-Bobaz Gulf) a quintic polynomial (i.e., of degree 5) is suitable to model the trend during the period 1993 to 2010. The order is evaluated by assessing the root mean square (RMS) values of the residuals. It was noticed that when increasing the order of the polynomial to higher than 5 , the RMS did not decrease significantly.

After the trend removal, LSSA (Eq. (5)) is implemented to the remaining part of the gauge observations and the other 280 satellite time-series to derive the main significant frequencies of the Caspian Sea. The details of the implementation are described in the following section (Sec 5.2).

5.2. SSH *frequencies*

In the *point-wise approach*, the spectrum of every observed point independently shows the local sea surface behavior. However, the periodic components originate from common sources. Space-borne measured instantaneous sea surface heights are the differences of satellite height and measured ranges (e.g., Eq. 2). Therefore, major periodic effects on SSH are due to;

- Seasonal and celestial tidal periodic effect on the measured ranges, or,
- Orbital periodic perturbations in the positions of satellite.

After removing the polynomial trend of the sample point height records, the residual observations are analyzed using LSSA (Eq. 5). As an example, the achieved power spectrum result related to the middle point of the Caspian Sea (shown in Fig. 3, middle), before correcting for the tidal frequencies, is demonstrated in Fig. 6. The validity level is derived from implementing the statistical test (Eq. 7).

FIGURE 6

Most of the computed power spectrum, from the 280 time-series, show a long wave-length 0.00022 cycle per day (cpd) frequency ($\approx$ 12.5 years), which passes the statistical test in (Eq. 7). The result corroborates the 12.8 years value found by Lyubushin et al. (2004) (see e.g., Fig. 6). The tidal frequencies are also clearly highlighted in the power spectrum of the signals. Of course, not all frequencies result from water level fluctuation.

Due to the sample rate (ν_s = 9.915965 days) of T/P and JASON-1, some aliased frequencies have emerged in the spectrum. For example, the aliased frequency of $\nu_a^{M_2} = 0.0161$ cpd ($\approx$ 62.107 days) is equivalent to the lunar semidiurnal frequency M_2 with $\nu^{M_2} = 1.9305$ cpd. S_2 corresponds to the Sun semidiurnal frequency with the aliased frequency of $\nu^{S_2} = 0.017024$ cpd as well as $\nu^{SA} = 0.002738$ cpd that corresponds to the Sun annual frequency with a period of 365.23 days. These 3 frequencies were found to be dominant tidal frequencies in most of the 280 time-series. Fig. 7 shows the amplitudes and phases of M_2 and S_2 to be compared with those of T-UGO model in Kouraev et al. (2011). Our results confirms the model outputs, specifically w.r.t their phases. however,

the derived amplitudes of M_2 and S_2 with the mean value of 4.2 and 2.8 cm, respectively, are bigger than the model outputs.

FIGURE 7

A summery of the major tidal frequencies and their computed aliased values corresponding to our point-wise LSSA are listed in Table (1). The results are comparable to those of experimental formula (Eq. (9)) provided by Wang (2004). The mean amplitude of each tidal frequency in the Caspian also is also reported in Table (1).

TABLE 1

To explore the effect of non-tidal perturbation forces in the level variation signals, after removing trend, we corrected the time-series for the long-wavelength ($\approx$ 12.5 years) and the tidal periodic components. This was done by assuming the tidal frequencies listed in Table 1 as known, then their effects were computed from Eq. (5) and removed from the time-series. As a result of this correction, short wavelength variations are superimposed on a long-term periodic fluctuation. In other words, the LSSA of the remaining parts visualize the unknown periodic constituents of the observed SSH if the omission error is neglected. For instance, Fig. 8 shows power spectrum of the sample point corresponding to Fig. 3 after removing the tidal components. A new peak that was already suppressed in total signal spectrum due to the significant effect of the tidal components emerges.

FIGURE 8

This new frequency is related to the periodic perturbation of the satellite height since nearly all the periodic tidal components are removed from SSH. Spectral analysis of the residual orbital height, i.e., satellite altitude minus nominal orbital (provided in MGDR and IGDR data) height minus tidal periodic effect, shows the same spectrum for the middle point in Fig. 1 (see Fig. 9A).

For the sake of completeness, the same analysis have been performed for two other satellite position above the Lake Victoria in East Africa (see the results in Fig. 9B) and the Atlantic ocean (in Fig. 9C). Their spectra are similar to the spectrum of the middle point above the Caspian Sea. Of course, a few more meaningful components are visible in the lake Victoria spectrum (compare the peaks in A, B and C) whose detail interpretation is outside the scope of this paper (see Fig. 9).

FIGURE 9

5.3. Global scheme of level variations within the Caspian Sea

After removing the orbital frequency from the previously corrected time-series, we interpolated the 280 time-series to monthly intervals covering 1993 to

2008.8. Then PCA was applied to extract the main spatio-temporal variability of the Caspian Sea level changes. Our results show that the first orthogonal components (EOF1 and PC1), corresponding to 91% of the level change variance, are significant while the remaining components correspond to noise (see Fig. 10). Spatial pattern of EOF1 indicates that the regions over the northern part of the Caspian Sea exhibit bigger amplitude of the level changes compared to the middle and south parts of the Sea. The temporal component (PC1) shows an annual cycle along with a trend which can be devided to 5 intervals, including 1993 to March 1995, April 1995 to September 1996, October 1997 to April 2001, June 2001 to December 2005 and January 2006 to October 2008. The mean value of the linear rates of level variations of the whole sea, corresponding to the mentioned time-intervals are found as 21.1 , -22.1 , -6.2 , 10.6 and -16.1 cm/year. The results confirm and extend that of Lebedev and Kostianoy (2006)'s study.

FIGURE 10

5.4. Relationship to the Volga River

To study the influence of the Volga River on the water level changes of the Caspian Sea, we considered the three points discussed previously (Fig. 1). The time-series are derived from the point-wise approach, selected from the pass 92 (Fig. 1). Sea surface height power spectrum of these points are depicted in Fig. (11). The most-northern point shows high fluctuations at high frequencies since the Caspian Sea is mostly fed by the Volga River discharge. The variations gradually changes to low-frequencies, which more or less show the local variations (see Fig. 11 and compare the amplitudes of the peaks).

FIGURE 11

Analysis of the Volga River discharge could be very useful for classifying the peaks that appeared in the SSH spectrum in Fig. (11). The SSH of the Volga River during $1992 - 2010$ along with the monthly record of the river outflow during $1999 - 2005$ is shown in Fig. (5). The spectral analysis of the Volga's SSH is given in Fig. (12). The spectrum shows the annual and semi annual frequencies are dominant in the discharge of Volga (Fig. (12, Top)). Removing these two peaks leads to an amplification of less prominent components, i.e., the frequencies of 0.0068 cycle per day (cpd), 0.0078 cpd, 0.0098 cpd and 0.0112 cpd emerge as the four significant peaks in Fig. (12, Bottom).

FIGURE 12

One can see that the SSH spectrum of the most northern point (Fig. 11, A) is very similar to Volga discharge spectrum (Fig. 12, Bottom). Furthermore, it is clearly seen that the fluctuation of the sea surface in the north has short period. However, the middle and southern parts of the sea experience the longer-period effects of the Volga River (Fig. 11, B and C). This is also confirmed from the computed cross-correlation of the Volga's power spectrum with the powers of

Fig. 11. The results indicate 0.63 , 0.51 and 0.4 of zero-lag correlation for the north, middle, and southern points, respectively.

To illustrate the effect of the Volga River on the Caspian Sea fluctuations during the study period, we computed the phase lag of the significant frequencies of the Volga River (Fig. 12, Bottom) from the sea surface height time-series along pass 92 (Fig. 1) as a function of distance from the north (Volga entrance). The results are plotted in Fig. 13. The process of the first three frequencies 0.00068 , 0.0078 and 0.0098 (cpd) respectively corresponding to the periods of 4.02 years, 128.2 days and 102 days appears to vary southwards. The phase lag of the 0.0112 cpd signal corresponding to 89 days (Fig. 13, D) is nearly constant in the same direction. Therefore, different locations experience the effect of the first three frequencies with a time delay, while the last component (0.0112 cpd) is visible simultaneously at different locations.

FIGURE 13

6. Conclusions

In this paper, we studied the frequency structure of the water level changes in Caspian Sea using point-wise measurements of T/P and Jason-1 altimetry missions. The computed 280 SSH time-series expand the previous studies to cover the surface of the Caspian Sea more appropriately. Further, they can also be useful for the water management of the Caspian Sea thus providing a tool to analyse each part of the sea individually, while the PCA would be useful for extracting the main spatial and temporal pattern of level variations within the sea. Our results also show the impact of the Volga River on the Caspian Sea level changes, thus corroborating the previous findings. A summary of the outcomes of this research are as follows:

- Long-term in-situ daily tide-gauge observations in the Anzali port (1983-2006) and most of the altimetry time-series contained a 12.5-years long-wavelength periodic component which passes the statistical significant test.
- The lssa of the ssh residuals time-series shows the presence of significant tidal frequencies that are aliased to other frequencies, from which M_2, S_2 and SA are dominant.
- The lssa of the satellite orbital heights time-series indicates some significant frequencies, which are also presented in the ssh power spectra.
- The results of PCA shows that the amplitude of water variations in the north part of the Caspian Sea is bigger than the middle and south parts of it.
- Analysis of point-wise time-series shows a phase differences between various passes. It seems that these differences are due to the distance of the

passes to the Volga River. Changes in the discharge from the Volga do not effect the entire sea immediately. Therefore, the locations that are closer to the river experience fluctuations in water level sooner than the more distant locations. Consequently, it seems that point-wise analysis is more suitable for investigating the water level changes in the Caspian Sea and the same may be said for other vase area inland water sources.

- Applying the LSSA to the level fluctuations of the Volga River indicates 5 major frequencies in addition to the annual and semi-annual frequencies. Studying the phase distribution of these frequencies shows their influences on the Caspian Sea level are location-dependent. These results confirm the findings of previous studies, e.g., Lebedev and Kostianoy (2006) and (2008a,b) thus showing the impact of Volga in the spectral structure of level variations of the Caspian Sea. Note, however, that there are also other external factors such as precipitation and evaporation that on one hand are high correlated to the out flow of the Volga River and on the other hand have considerable high influence on the level variations of the Caspian Sea (see e.g., Kouraev et al., 2011). Therefore, the reported frequencies might change w.r.t the changes of climatic factors.

- Annual, semi-annual and seasonal frequencies are clearly visible in the Caspian Sea. Moreover, there is a c.a. 0.0009 cpd frequency (corresponding to the period of 3 years) in both SSH and tide-gauge time-series. Interpretation of this frequency is still an open question.

Acknowledgement

The authors thank the two anonymous reviewers and the editor J. Lastovicka for their helpful remarks which improved considerably the manuscript. We also thank K. Fleming (GFZ, Potsdam) and S. Dodge (Ohio State University) for their comments and proofreading of the original version of this article. M.A. Sharifi is grateful for funding from the Deutscher Akademischer Austausch Dienst (DAAD) through award A/08/00069. J.L. Awange acknowledges the financial support of a Curtin Research Fellowship and the Alexander von Humboldt (Ludwig Leichhardt Memorial Fellowship) Foundation that supported his time at Curtin University and Karlsruhe Institute of Technology (KIT), respectively. E. Forootan would like to thank Bonn University for the financial support. The altimetry data sets used in this study are derived from:

ftp://podaac-ftp.jpl.nasa.gov/allData/topex/L1B

ftp://podaac-ftp.jpl.nasa.gov/allData/jason1/L2/gdr_c

http://www.legos.obs-mip.fr/en/soa/hydrologie/hydroweb/Page_2.html

References

AVISO, 1996. User Handbook - Merged TOPEX/Poseidon Products (GDR-M). AVI-NT-02-101-CN, Ed. 3.0, July 1996.

Awange, J.L., Ogalo, L., Bae, K.H., Were, P., Omondi, P., Omute, P., Omullo, M., 2008. Falling lake Victoria water levels: is climate a contributing factor? J. Climatic Change, 89, 281-297, doi:10.1007/s10584-008-9409-x.

Benada, J.R., 1997. TOPEX/POSEIDON Generation B (MGDR-B) User's Handbook, Version 2.0. Technical report, Physical Oceanography Distributed Active Archive Center (PODAAC), Jet Propulsion Laboratory, California Institute of Technology.

Bird, E.C.F., 2010. Iran-Caspian Sea coast. Springer Netherlands, 861-866, doi:http: //dx.doi.org/10.1007/978-1-4020-8639-7_149.

Birkett, C.M., 1994. Radara altimetry: new concept in monitoring lake level changes. EOS, 75, 273-275, doi:10.1029/94EO00944.

Birkett, C.M., 1995. The contribution of TOPEX/POSEIDON to the global monitoring of climatically sensitive lakes. Journal of Geophysical Research 100, 25179-25204, doi:10.1029/95JC02125.

Brown, S., 2010. A novel near-land radiometer wet path delay retrieval algorithm: application to the Jason-2/OSTM advanced microwave radiometer. IEEE Trans. Geosci. Remote Sens., vol. 48, no. 4, 1986-1992.

Cartwright, D., 1993. Satellite altimetry in geodesy and oceanography: theory of ocean tides with application to altimetry. Springer Berlin / Heidelberg, pp. 100-141, doi:http: //dx.doi.org/10.1007/BFb0117927.

Cazenave, A., Bonnefond, P., Dominh, K., Schaeffer, P., 1997. Caspian Sea level from TOPEX/POSEIDON altimetry: Level now falling. Geophysical Research Letters 24 (8), 881-884, doi:http: //dx.doi.org/10.1029/97GL00809.

Cazenave, A., Schaeffer, P., Berge, M., Brossier, C., Dominh, K., Gennero, M.C., 1996. High-resolution mean sea surface computed with altimeter data of ERS-1 (geodetic mission) and TOPEX/POSEIDON. Geophysical Journal International, 125, 696-704, doi:10.1111/j.1365-246X.1996.tb06017.x.

Chatfield, C., 1989. The analysis of time series: an introduction. Chapman and Hall, pp. 352, ISBN-10:1584883170.

Chambers, D.P., Ries, J.C., Urban, T.J., 2003. Calibration and Verification of Jason-1 Using Global Along-Track Residuals with TOPEX Special Issue: Jason-1 Calibration/Validation. Marine Geodesy, 26 (3-4), doi:10.1080/714044523.

Crétaux, J-F., Birkett, C., 2006. Lake studies from satellite radar altimetry. Comptes Rendus Geosciences, 338 (14-15), 1098-1112, doi:10.1016/j.crte.2006.08.002.

Crétaux, J-F., Jelinski, W., Calmant, S., Kouraev, A., Vuglinski, V., Bergé Nguyen, M., Gennero, M-C., Nino, F., Abarca Del Rio, F., Cazenave, A., Maisongrande, P., 2011. SOLS: A lake database to monitor in near real time water level and storage variations from remote sensing data, Journal of Advanced Space Research, 1497-1507, doi:10.1016/j.asr.2011.01.004.

Craymer, M., 1998. The least squares spectrum, its inverse transform and autocorrelation function: theory and some applications in Geodesy. PhD thesis, University of Toronto, Canada.

Dumont, H.J., 1998. The Caspian Lake: history, biota, structure, and function. Limnnology and Oceanography 43, 44-52, ISSN:0024-3590.

Dumont, H.J., Tamara, A., Shiganova, U.N., 2004. Aquatic invasions in the Black, Caspian, and Mediterranean Seas (Nato Science Series). Kluwer Academic Publishers, pp. 313, ISBN-10:140201869X.

Foster, G., 1996. Time series analysis by projection. I. statistical properties of Fourier analysis. Astronomical Journal 111, pp. 541-554, doi:10.1086/117805.

Georgievskiy, V.Y., 2001. A review and critical analysis of the methods and results of the Caspian Sea level forecasts, developed for 5 to 10 and 20 to 100 years horizons. Technical report, CEP. www.caspianenvironment.org/report_miscell2.htm (access date: 20.05.2008).

Gil, E., de Toro, C., 2005. Improving tide-gauge data processing: A method involving tidal frequencies and inverted barometer effect. Comput. Geosci., 31, 1048-1058, doi:10.1016/j.cageo.2005.02.006.

Hwang, C., Peng, M.F., Ning, J., Luo, J., Sui, C.H., 2005. Lake level variations in China from TOPEX/Poseidon altimetry: data quality assessment and links to precipitation and ENSO. Geophysical Journal International 161, 1-16, doi:10.1111/j.1365-246X.2005.02518.x.

Ignatov, Ye.I., Kaplin, P.A., Lukyanova S.A., Solovieva, G.D., 1993. Evolution of the Caspian Sea coasts under conditions of sea-level rise: model for coastal change under Increasing "Greenhouse Effect". Journal of Coastal Research 9 (1), 104-111, ISSN:0749-0208.

Kosarev, A.N., Yablonskaya, E.A., 1994. The Caspian Sea. The Netherlands: SPB Academic Publishing, pp. 260, ISBN-10:9051030886.

Kosarev, A.N., 2005. Physico-Geographical Conditions of the Caspian Sea. The Handbook of Environmental Chemistry, Volume 5P, pp. 5-31, doi:10.1007/698_5_002.

Kostianoy, A.G., Lebedev, S.A., 2006. Satellite altimetry of the Caspian Sea. 15 Years of Progress in Radar Altimetry Symposium. Venice Lido, Italy, 13-18 March 2006, http://www.iki.rssi.ru/earth/articles06/vol2-113-120.pdf (access date: 30.11.2010).

Kouraev, A.V., Papa, F., Buharizin, P.I., Cazenave, A., Crétaux, J.-F., Dozortseva, J., Rémy, F., 2003. Ice cover variability in the Caspian and Aral seas from active and passive microwave satellite data. Polar Res., 22, 43-50.

Kouraev, A.V., Papa, F., Mognard, N.M., Buharizin, P.I., Cazenave, A., Crétaux, J.-F., Dozortseva, J., Rémy, F., 2004. Sea ice cover in the Caspian and Aral Seas from historical and satellite data. Journal of Marine Systems, 47 (1-4), 89-100, doi:http://dx.doi.org/10.1016/j.jmarsys.2003.12.011.

Kouraev, A.V., Shimaraev, M.N., Buharizin, P.I., Naumenko, M.A., Crétaux, J.-F., Mognard, N.M., Legrésy, B., Rémy, F., 2008. Ice and snow cover of continental water bodies from simultaneous radar altimetry and radiometry observations. Surveys in Geophysics, 29 (4-5), 271-295, doi:10.1007/s10712-008-9042-2.

Kouraev, A.V., Crétaux, J.-F., Lebedev, S.A., Kostianoy, A.G., Ginzburg, A.I., Sheremet, N.A., Mamedov, R., Zakharova, E.A., Roblou, L., Lyard, F., Calmant, S., Berge-Nguyen, M., 2011. Satellite altimetry applications in the Caspian Sea (Chapter 13). In Coastal Altimetry, (Eds) S., Kostianoy, A., Cipollini, P., and Benveniste, J. Springer, 331-366, ISBN:978-3-642-12795-3.

Lebedev, S.A., Kostianoy, A.G., 2005. Satellite Altimetry of the Caspian Sea. Moscow: Sea, 2005, pp. 366 (in Russian).

Lebedev, S.A., Kostianoy, A.G., 2006. The Caspian Sea level, dynamics, wind, waves and uplift of the Earth's crust derived from satellite altimetry. Proc., ISRS 2006 PORSEC Conference, BEXCO, Busan, Korea, 2-4 November 2006, 973-976.

Lebedev, S.A., Kostianoy, A.G., 2008a. Investigation of the Caspian Sea Surface Dynamics Based on the Satellite Altimetry and Drifter Data. Abstracts, 37th COSPAR Scientific Assembly Montreal, Canada, 13-20 July 2008, Abstract CD, ISSN:1815-5619, A21-0033-08.

Lebedev, S.A., Kostianoy, A.G., 2008b. Integrated using of satellite altimetry in investigation of meteorological, hydrological and hydrodynamic regime of the Caspian Sea. Journal of Terrestrial Atmospheric and Oceanic Sciences, 2008, 19, 71-82.

Lebedev, S.A., Kostianoy, A.G., 2010. Complex investigation of meteorological, hydrological and hydrodynamic regime of the Caspian Sea based on satellite altimetry data. Proc. Int. Symp. "Oceans from Space", 26-30 April 2010, Venice, Italy, 149-150.

Lyubushin, A.A., Gelder, P.H.A.J.M., Bolgov, M.V., 2004. Spectral analysis of Caspian level variations. In Proceedings of the 23rd International Conference on Off-shore Mechanics and Arctic Engineering, June 20-25, Vancouver, British Columbia, Canada. 108-110, ISBN:90-805649-9-0.

Mercier, F., Zanife, O.-Z., 2006. Improvement of the Topex/Poseidon altimetric data processing for hydrological purposes (CASH project). Proceedings of the symposium on 15 years of Progress in Radar Altimetry 13-18 March 2006 Venice, Italy.

Minster, J.F., Brossier, C., Rogel, P., 1995. Variation of the mean sea level from TOPEX/POSEIDON data. Journal of Geophysical Research 100, 25153-25161, doi:10.1029/95JC02304.

Nerem, R.S., 1995. Measuring global mean sea level variation using TOPEX/POSEIDON altimeter data. Journal of Geophysical Research 100, 25135-25151, doi:10.1029/95JC02303.

Nerem, R.S., Putney, B.H., Marshall, J.A., Lerch, F.J., Pavlis, E.C., Klosko, S.M., Luthcke, S.B., Patel, G.B., Williamson, R.G., Zelensky, N.P., 1993. Expected orbit determination performance for the TOPEX/Poseidon mission. Geoscience and Remote Sensing, IEEE Transactions 31, 333-354, doi:10.1109/36.214910.

Picot, N., Case, K., Desai, S., Vincent, P., 2003. AVISO and PODAAC User Handbook. IGDR and GDR Jason Products. SMM-MU-M5-OP-13184-CN (AVISO), JPL D-21352(PODAAC).

Preisendorfer, R. 1988. Principal component analysis in Meteorology and Oceanography. Elsevier: Amsterdam, 426 pages. ISBN:0444430148

Rodionov, S.N., 1994. Global and regional climate interaction: The Caspian Sea experience (Springer), pp. 256. ISBN-10:0792327845.

Rubin, D.B., 2002. Statistical analysis with missing data. Wiley, New York, pp. 408, ISBN-10:0471183865.

Shannon, C., 1984. Communication in the presence of noise. Proceedings of the IEEE, 72, 1192-1201, doi:10.1109/PROC.1984.12998.

Shum, C.K., Cheng, Y.Yi., Kuo, C., Braun, A., Calmant, S., Chambers, D., 2003. Calibration of Jason-1 altimeter over lake Erie. Mar. Geod. 26 (3-4), 335-354, doi:10.1080/714044525.

Steeves, R.R., 1981. A statistical test for significance of peaks in the least squares spectrum. In Collected Papers of the Geodetic Survey. Department of Energy, Mines and Resources, Surveys and Mapping, Ottawa, 149-166.

Swenson, S., Wahr, J., 2007. Multi-sensor analysis of water storage variations of the Caspian Sea. Geophysical Research Letters 34, L16401, doi:10.1029/2007GL030733.

TDA, 2002. Trans boundary diagnostic analysis for the Caspian Sea. The Caspian Sea environment programme 2002. http://www.caspianenvironment.org (access date: 31.10.2010).

Vaníček, P., 1969. Approximate spectral analysis by Least-Squares Fit. Successive spectral analysis. Astrophysics and Space Science, 4, 387-391, doi:10.1007/BF00651344.

Vaníček, P., Krakiwsky, E., 1986. Geodesy the concepts. New York: Elsevier science publishing, pp. 697, ISBN-10:0444877770.

Vityazev, V.V., 1996. Time series analysis of unequally spaced data: Intercomparison between the Schuster periodogram and the LS-spectra. Astronomical and Astrophysical Transactions: The Journal of the Eurasian Astronomical Society 11, 139-158, doi:10.1080/10556799608205461.

Wang, Y., 2004. Ocean tide modeling in southern ocean. Technical report 471, Department of civil and Environmental Engineering and Geodetic Science, The Ohio State University.

Wells, D., Vaníček, P., Pagiatakis, S., 1985. Least squares spectral analysis revisited, Lecture notes. Department of Geodesy and Geomatics Engineering, University of New Brunswick (UNB), http//gge.unb.ca/Pubs/TR84.pdf (access date: 31.10.2010).

Wu, D. L., Hays, P., Skinner, W., 1995. A least squares method for spectral analysis of space-time series. Journal of the Atmospheric Sciences 52, 3501-3511, doi:10.1175/1520-0469(1995)052<3501:ALSMFS>2.0.CO;2.

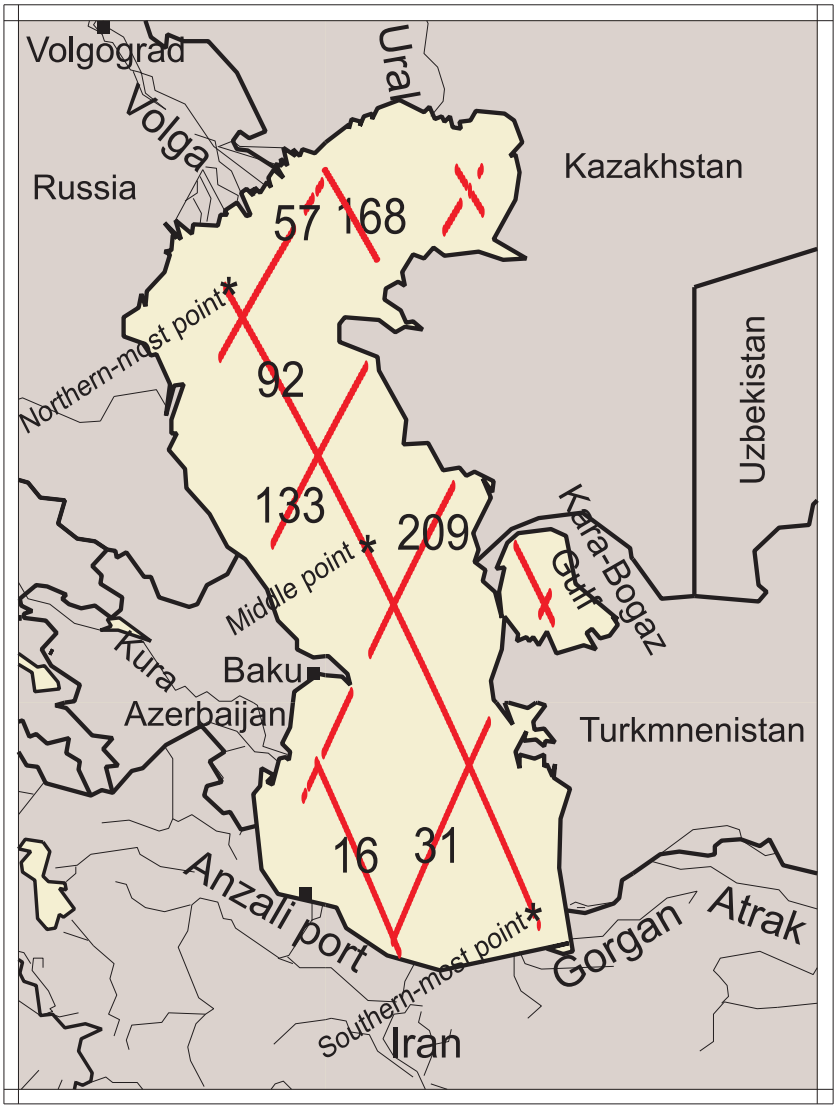

Figure 1: The Caspian Sea and its surrounding regions. Figure shows the ground-tracks of T/P and JASON-1 within the Caspian Sea.

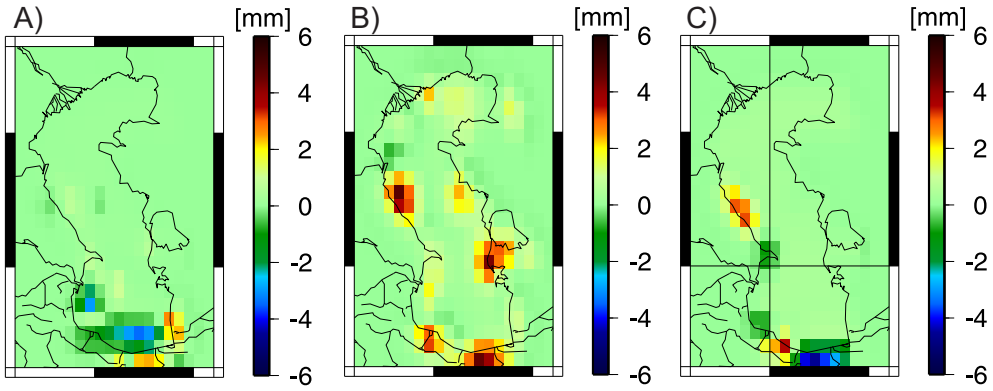

Figure 2: Difference between standard deviation of the original (used in this study) and ECMWF-derived corrections including, A) dry tropospheric, B) wet tropospheric, and C) inverse barometric corrections.

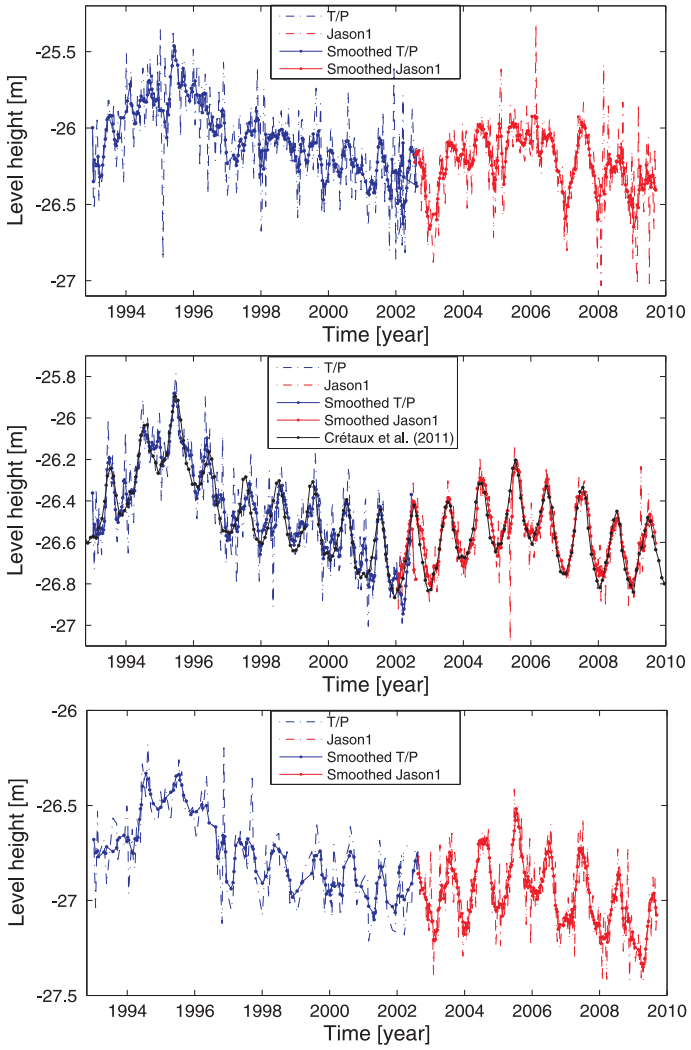

Figure 3: Point-wise SSH variations of the three sample points shown as the northern-most, middle and southern-most points in Fig. 1, during the period 1993–2010. Top: the time-series of the Northern-most point that is located in 44.86 °N and 48.01 °E, near to the Volga River entrance. Middle: the time-series of the Middle point, located in 42.28 °N and 50.16 °E. For comparison, the results of Crétaux et al. (2011) for a virtual point located in 42 °N and 50 °E is also shown with the solid black line (see http://www.legos.obs-mip.fr/en/soa/hydrologie/hydroweb/StationsVirtuelles/SV_Lakes/Caspian.html). Bottom: the time-series of the Southern-most point that is located in 37.59 °N and 53.54 °E.

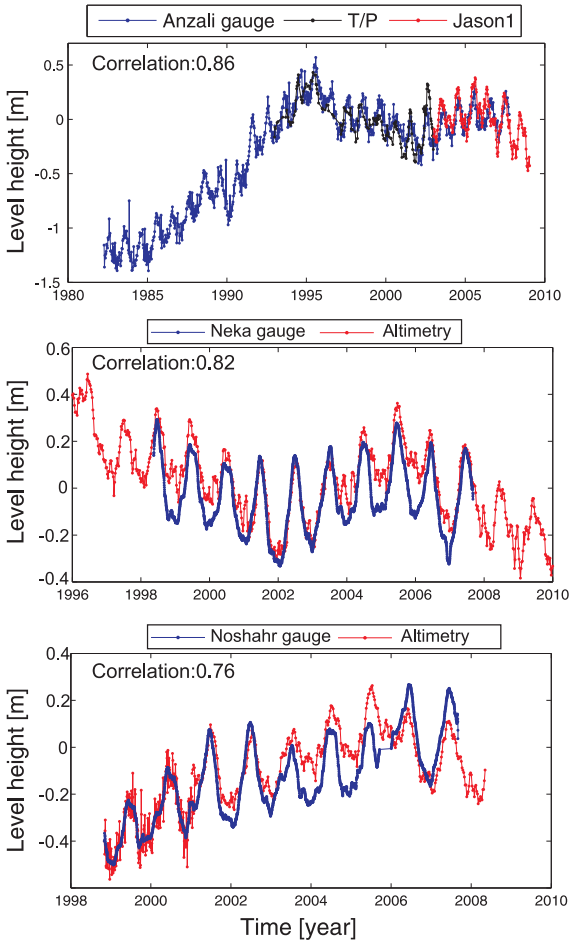

Figure 4: (top) The Anzali gauge (located at 37.47 °N and 49.46 °E) records during 1983–2006, smoothed with a 10-days low-pass filter is shown with the solid blue line. The SSH time-series derived from T/P and JASON-1 corresponding to a virtual location (along the pass 16, see Fig. 1) with latitude 37.54°N and longitude 50.74°E are shown with the solid black and red lines, respectively. The figure also shows the comparisons between tide gauge observation in (middle) Neka (36.84 °N and 53.27 °E) as well as (bottom) in Noshahr (36.65 °N and 51.50 °E) and those of altimetry.

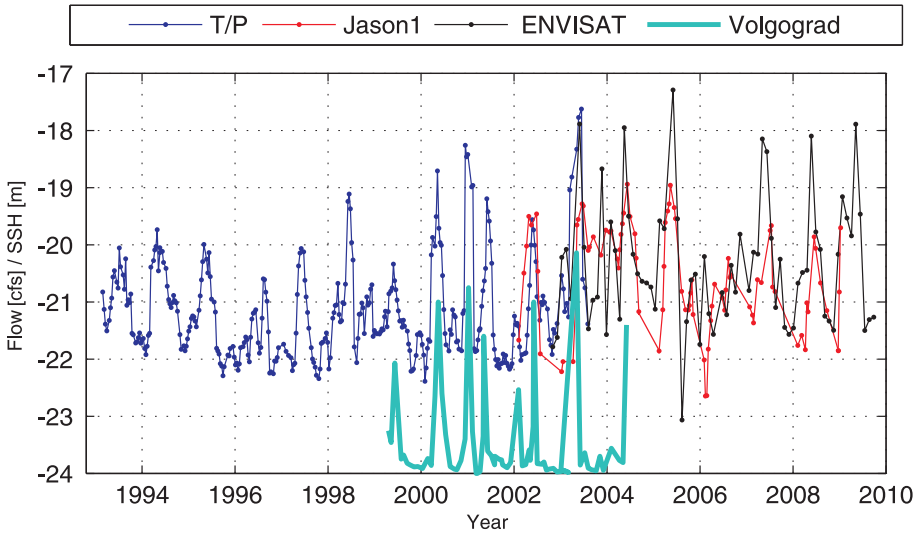

Figure 5: SSH variations of the Volga River (located close to the Volgograd power station, in 44.67°E and 48.82°N) derived from T/P altimetry (1992 - middle 2002, in blue line), JASON-1 (middle 2002 to September 2009, in red), ENVISAT product, located in 45.61°E and longitude: 48.44°N (2002 - 2010, in back), and the monthly water discharge at the Volgograd power station in cubic feet per second (cfs) during 1999–2005 in green. The time-series of ENVISAT was derived from the LEGOS website (http://www.legos.obs-mip.fr/en/soa/hydrologie/hydroweb/Page_2.html)

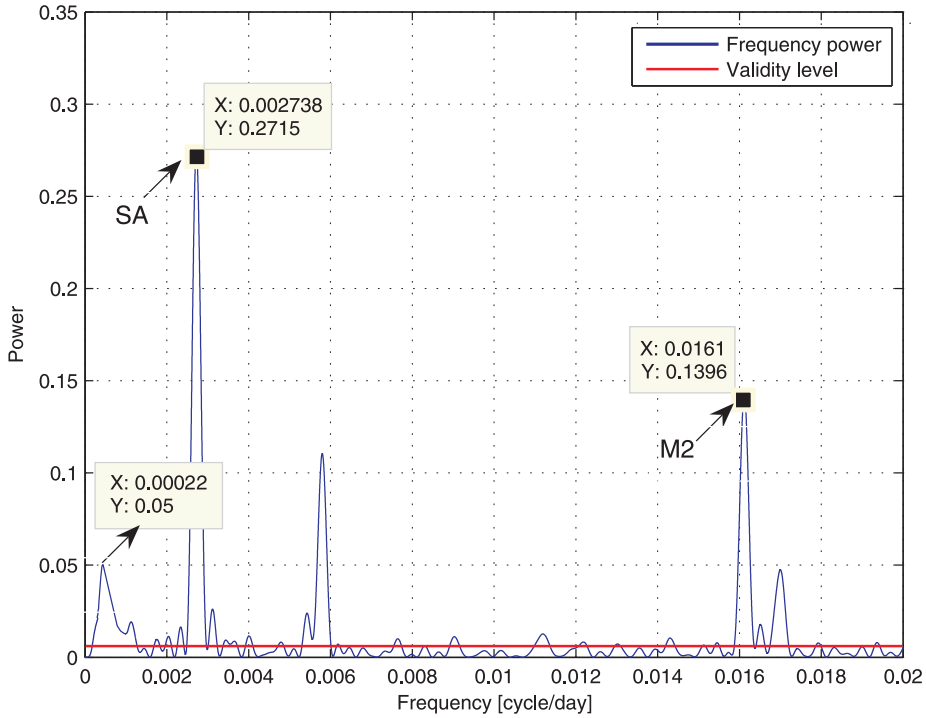

Figure 6: Power spectrum of the detrended SSH of the sample point's record (Fig. 3). In this figure $M2$ stands for lunar semidurnal frequency and SA is for the Sun annual frequency. A short 0.00022 cycle per day (cpd) frequency ($\approx$ 12.5 years) which was reported in Lyubushin et al. (2004) (as a 12.8 years frequency) is also found in our analysis.

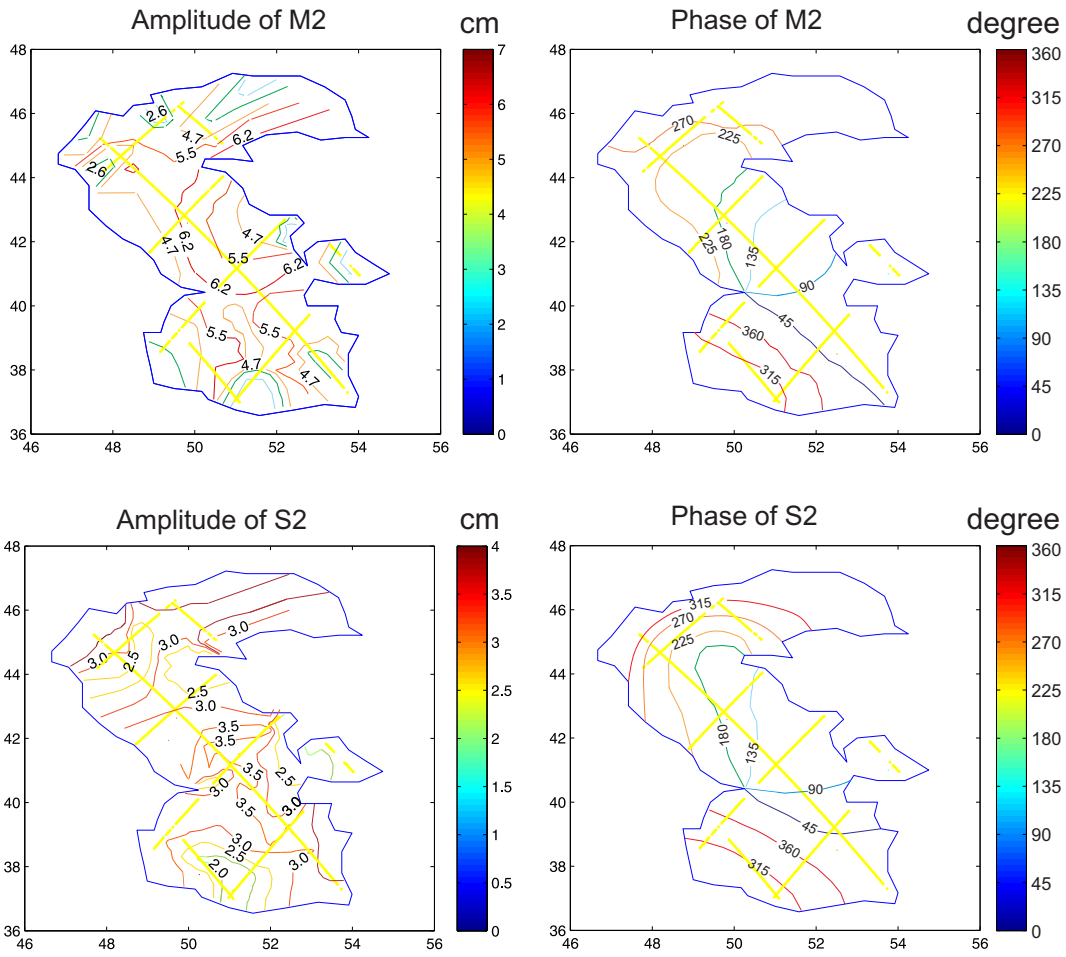

Figure 7: Amplitude and phase of the M_2 (2 graphs on top) and S_2 (2 graphs on bottom). The results are derived by implementing LSSA (Eq. (5)) on the 280 virtual time-series of T/P and JASON-1

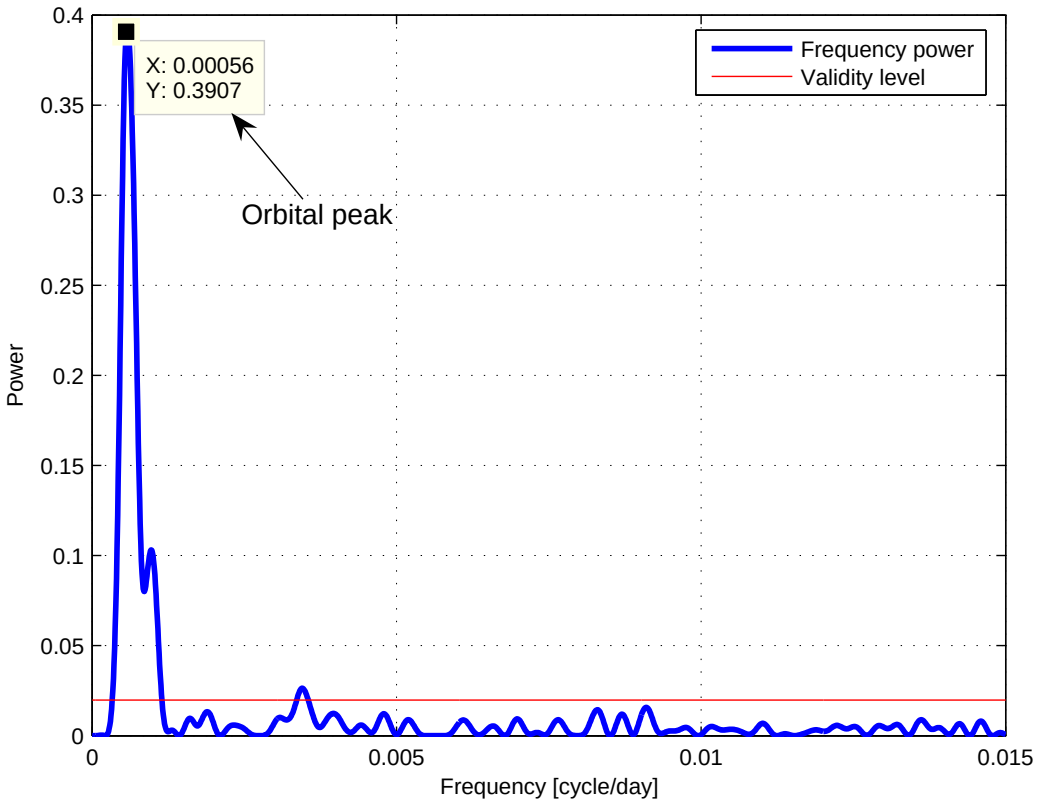

Figure 8: The sample point (Fig. 3) SSH spectrum after removing the tidal components

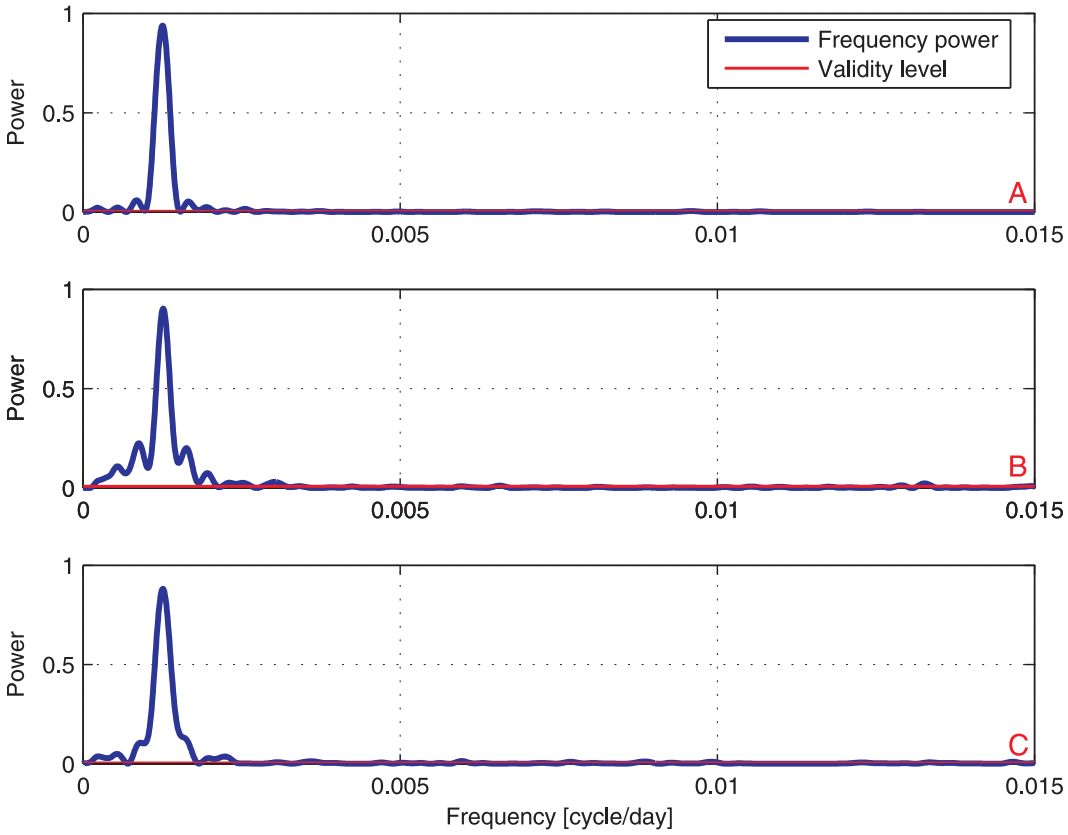

Figure 9: Power spectrum of satellite height time-series at three different sample points above: A) the Caspian Sea, B) Lake Victoria and C) the Atlantic Ocean. The spectra all shows a similar pattern

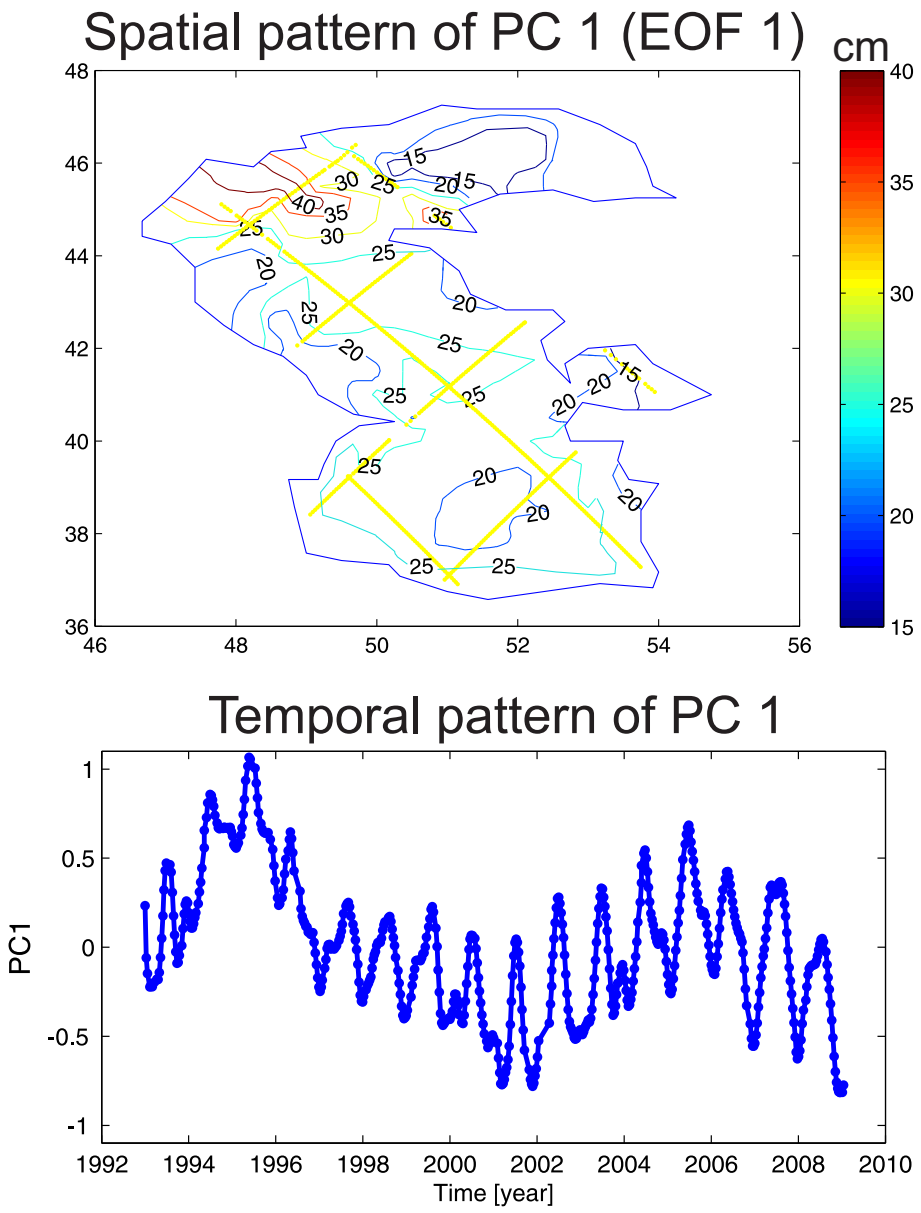

Figure 10: Results of PCA, applied on the 280 tidal and orbital corrected time-series: top) the spatial pattern in cm and bottom) its corresponding temporal pattern which is scaled being between +1 and -1. Multiplying EOF1 by PC1 using (Eq. 7), one can reconstruct 91% of level changes in the Caspian Sea.

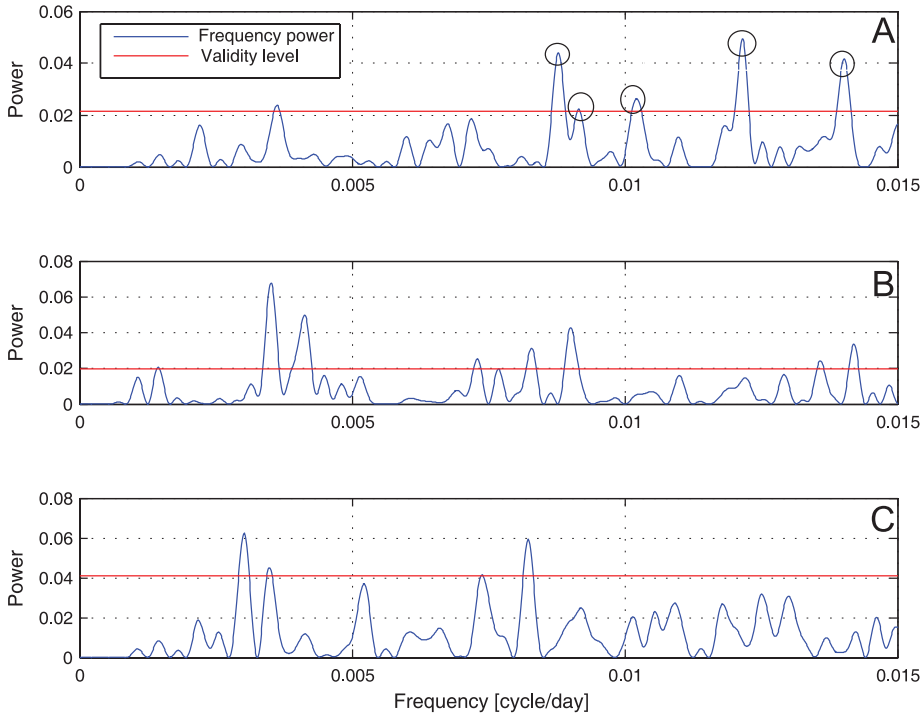

Figure 11: Power spectrum of three northern-most, middle and southern-most points in the Caspian Sea (Fig. 3), after removing trend, tidal orbital frequencies A) a sample point located near the Volga River entrance (44.86 °N, 48.01 °E), B) a point in the middle of the Caspian Sea (42.28 °N, 50.16 °E) and C) a point in the south of the Caspian Sea (37.59 °N, 53.54 °E).

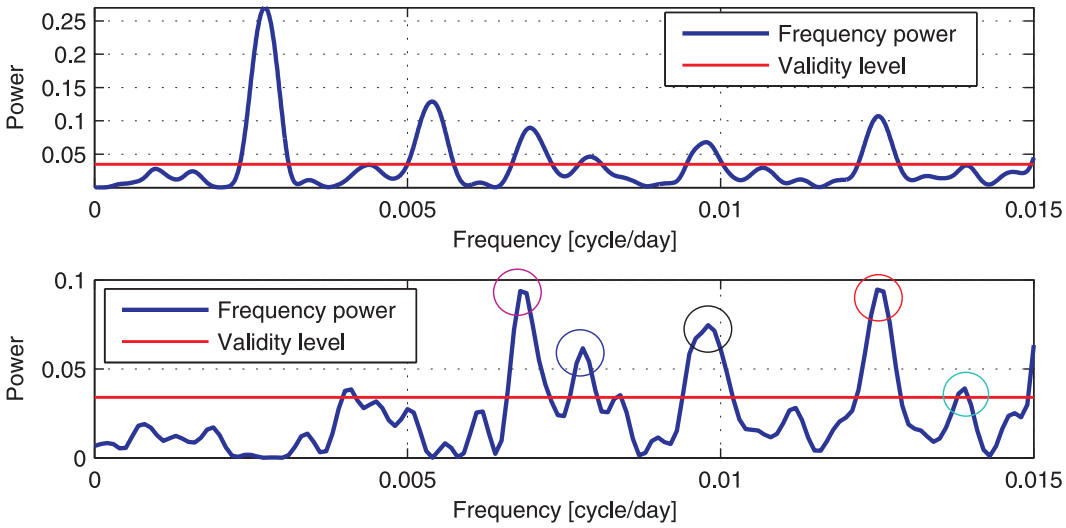

Figure 12: Top: Power spectrum of the SSH over the Volga River which is shown in Fig. 5 after linear de-trending. Bottom: Power spectrum of the Volga River without annual and semi-annual frequencies.

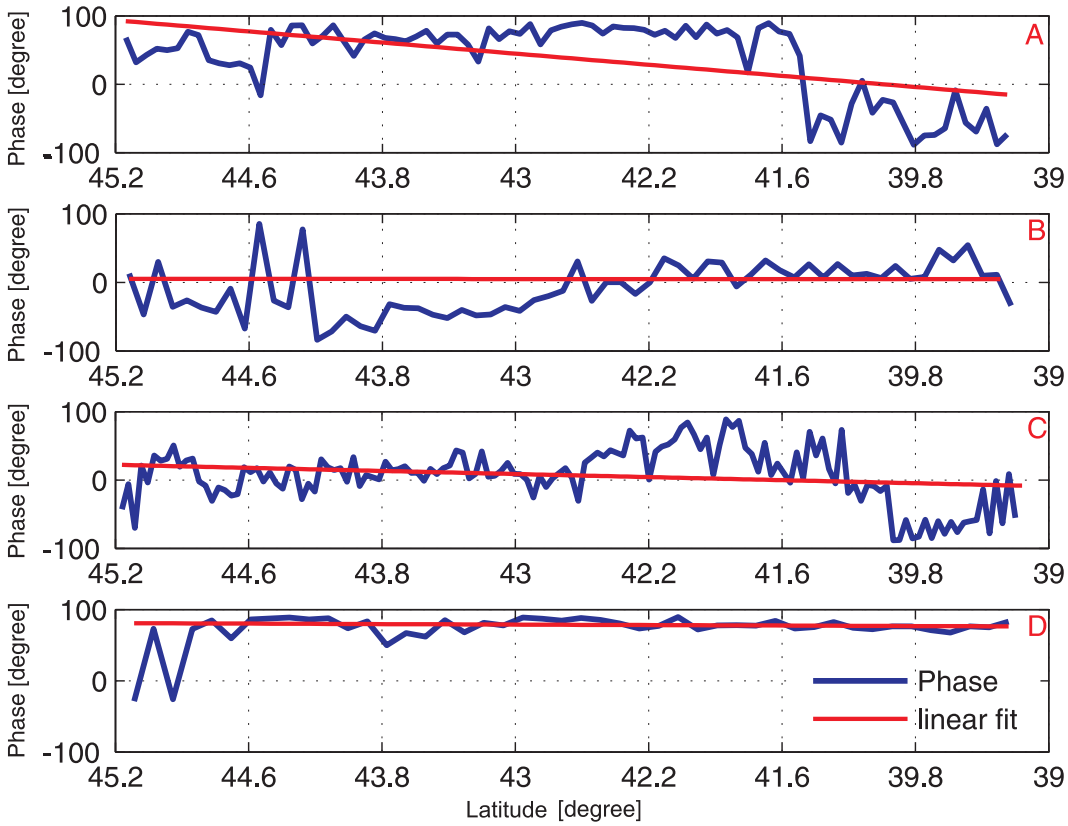

Figure 13: Effect of the Volga River on the Caspian Sea level fluctuations showing the southward phase variation of the Volga River related SSH the: A) 0.0068 cpd, B) 0.0078 cpd, C) 0.0098 cpd and D) 0.0112 cpd frequencies.

Table 1: Main tidal components and their aliased frequencies. The first column indicates the sign of tidal frequencies, the second column the real value of the tidal frequencies derived from astronomical studies (c.f. Cartwright, 1993), the third column shows the corresponding real period, fourth column lists the computed frequencies with respect to T/P sampling rate, the fifth column is their corresponding aliased periods, and the sixth column the mean amplitude of the frequencies for the whole sea.

Sign	Frequency (cpd)	Period (day)	Aliased Frequency (cpd)	Aliased Period (day)	Mean Amplitude (cm)
SA	0.002738	365.260	0.002738	365.260	2.1
SSA	0.005476	182.621	0.005476	182.621	1.6
MSM	0.031435	31.812	0.031435	31.812	0.6
MM	0.036292	27.555	0.036292	27.555	0.4
MSF	0.067726	14.765	0.033125	30.189	0.3
MF	0.073202	13.661	0.027649	36.168	0.5
Q_1	0.893244	1.120	0.014417	69.365	0.7
O_1	0.929536	1.076	0.021875	45.714	1.2
P_1	0.997262	1.003	0.011250	88.891	0.2
S_1	1.000000	1.000	0.008512	117.485	1.4
K_1	1.002738	0.997	0.005774	17./192	2.0
O_2	1.859071	0.538	0.043750	22.857	0.2
N_2	1.895982	0.527	0.020191	49.528	0.2
M_2	1.932274	0.518	0.016101	62.107	4.2
S_2	2.000000	0.500	0.017024	58.742	2.8
K_2	2.005476	0.499	0.011548	86.596	0.2
M_3	2.898410	0.345	0.026274	38.061	0.2
M_4	3.864547	0.259	0.032202	31.054	0.2
S_4	4.000000	0.250	0.034047	29.371	0.2
M_6	5.796821	0.173	0.048303	20.702	0.1
S_6	6.000000	0.167	0.049780	20.088	0.1
M_8	7.729094	0.129	0.036447	27.437	0.1